

Thermoelectric evidence of the electronic structure changes from the charge-density-wave transition in FeGe

Kaila Jenkins¹, Yuan Zhu¹, Dechen Zhang¹, Guoxin Zheng¹, Kuan-Wen Chen¹, Aaron Chan¹,
Sijie Xu^{2,3}, Mason L. Klemm^{2,3}, Bin Gao^{2,3}, Ming Yi^{2,3}, Pengcheng Dai^{2,3}, and Lu Li^{1*}

¹*Department of Physics, University of Michigan, Ann Arbor, MI 48109, USA.*

²*Department of Physics and Astronomy, Rice University, Houston, TX 77005, USA.*

³*Rice Laboratory for Emergent Magnetic Materials and Smalley-Curl Institute, Rice University, Houston, TX 77005, USA.*

(Dated: August 27, 2025)

Kagome metals provide a material platform for probing new correlated quantum phenomena due to the naturally incorporated linear dispersions, flat bands, and Van Hove singularities in their electronic structures. Among these quantum phenomena is the charge density wave (CDW), or the distortion of the lattice structure due to the motion of correlated electrons through the material. CDWs lower the energy of the compound, creating an energy gap that facilitates behaviors akin to superconductivity, nonlinear transport, or other quantum correlated phenomena. The kagome metal FeGe has been shown to host a CDW transition at approximately 100 K, and its occurrence is strongly influenced by the sample annealing conditions. However, a notable gap in the literature is the lack of clear thermoelectric transport evidence for electronic structure changes associated with this CDW transition. Here we present evidence of electron behavior modification due to annealing disorder via thermoelectric measurements on FeGe crystals presenting a CDW transition and those without a CDW. The observed Nernst effect and Seebeck effect under sufficient annealing demonstrate modified electrical transport properties resulting from induced disorder, including a change in carrier sign and an enhancement of the Nernst effect due to the CDW. Our results provide evidence of multiple phase transitions, which confirms the influence of CDW on the thermal properties of FeGe and demonstrates the suppression of CDW with sufficient disordering.

Novel electronic and magnetic materials have garnered considerable interest in recent years because of their environmental, technological, and practical benefits. In particular, novel thermoelectric materials are materials that exhibit enhanced and attractive thermoelectric behaviors [1] such as higher electrical conductivity, lower thermal conductivity, or generally unique thermoelectric signatures such as the anomalous Nernst effect found in strongly spin-orbit-coupled materials [2–8]. The Nernst effect [9–11] provides evidence of mobile vortices in superconductors [12–15]. Fundamentally, the quasiparticle thermopower (Seebeck effect) provides a different test of the carrier types [16], and the quasiparticle Nernst effects are observed in semimetals with small Fermi surfaces [17]. The thermoelectric effect thus provides unique insight into the underlying physical properties of kagome materials [18, 19] and other strongly correlated electron materials [20].

The kagome material FeGe (the B35 phase) was reported to host a CDW transition around 100 K in the antiferromagnetic phase [21–24]. Evidence for this transition has been observed with scanning tunneling microscopy [22], photoemission spectroscopy [23, 25, 26], magnetic susceptibility, heat capacity, and the electrical transport measurements [21]. There is also a strong spin-lattice-charge coupling across the CDW transition [27]. The amorphous and thin film of the cubic (the B20 phase) FeGe samples have been reported to exhibit the anomalous Hall effect [28, 29]. However, the anomalous Hall effect in kagome lattice FeGe was only found at a temperature well below the CDW transition, where incom-

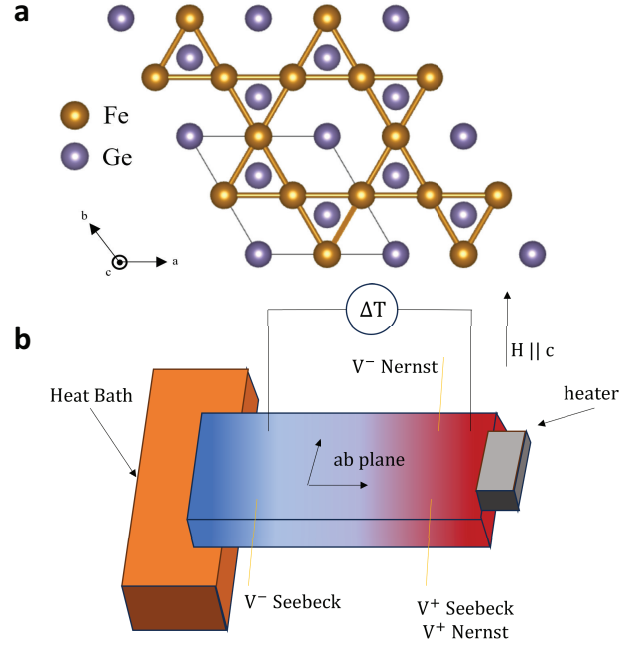


FIG. 1: (a) Crystal structure of Kagome magnet FeGe. (b) Experimental configuration for FeGe thermoelectric measurement. Gold leads indicate electrical contacts, with the sign convention labeled. The sample is oriented with the magnetic field applied along the crystal c -axis.

mensurate magnetic order was established below T_{cant} ($T_{cant} < T_{CDW}$) [30–35]. In addition, the suppressibility of CDW in kagome FeGe has been investigated, specifically with regard to annealing-induced CDW suppression and its effects on magnetic ordering [32–35].

However, despite the evidence for unique thermoelectric behavior in other topological and kagome compounds [36–42], Weyl materials [48–50], and evidence of anomalous Nernst effects and novel thermoelectric behavior in various ferrous materials [43–47], no other studies have published observations regarding the unique thermal features linked to the charge and magnetic ordering present in this compound. In particular, a question remains as to whether there are any sharp features in transport properties associated with the transitions. This letter seeks to fill this gap. Additionally, this work seeks to identify the role of disorder in both thermal behavior and magnetic ordering, as disorder has been shown to influence Nernst effects [51]. We report the finding of a strong Nernst effect in kagome FeGe, providing evidence of its features for the proposed CDW. We demonstrate here that kagome FeGe exhibits evidence of a charge density wave in thermopower measurements and a strong Nernst effect, and that this behavior is strongly suppressed when CDW order is removed through the process of high temperature annealing [32–35]. We also provide evidence here for magnetic disordering when the CDW feature is suppressed.

Single crystals were grown using Sn flux, and then annealed in separate batches under different temperature conditions. One batch was annealed at 320 °C for 96 hours, and another batch was annealed at 560 °C for 96 hours [35]. The orientation of the annealed samples was confirmed using X-ray diffraction. Samples were cut and polished to approximately 1 mm x 0.5 mm x 0.1 mm, perpendicular to the c -axis, and each was mounted on a copper block as a heat bath. Thermocouple type-E wires and gold-wire electrical contacts were mounted along the a - b plane. The negative Constantan leads were electrically shorted together. A 1 k Ω resistor was mounted on top of the sample to provide the necessary heat gradient for the measurement, and a layer of thermal epoxy was applied between the sample and the heater to prevent electrical contact. Each lead was mounted to its own nylon pillar using silver epoxy, and the electrical and thermal contacts were made to the PPMS puck using silver paint. Thermal epoxy was applied to each of the thermocouple joints, which were adhered to the sample without making electrical contact. This experimental setup is illustrated in Fig. 1, along with the FeGe crystal structure.

Measurements were taken using a Quantum Design Physical Property Measurement System (PPMS) Dynacool with a maximum field of 14 T. The magnetic field is oriented normal to the crystal plane surface. In FeGe, a square wave current excitation with an amplitude of 1.6

mA and a frequency of 0.04 Hz was utilized to energize the heater. The Nernst effect is measured perpendicular to the direction of the temperature gradient, and the Seebeck effect is measured along the direction of the temperature gradient. Each thermoelectric voltage signal was obtained by subtracting the bottom, heater-off signal, from the top, heater-on signal. The experiment for each sample consisted of several fixed-temperature field sweeps, varying the temperature in 5 K increments until after the anticipated 100 K charge density wave, and then with a slightly coarser temperature granulation after this feature.

The signal evolution of both the Seebeck signal, S_{xx} and Nernst signal, S_{xy} , for both conditions as a function of temperature and magnetic field are shown in Fig. 2. As can be noted in 2a, the thermopower signal shows two distinctive features under magnetic fields, one occurring around 6 T and the other around 9 T. Comparing it with the early report, we identify these features as the spin-flop transitions [32, 35]. These features appear to be present in the 320 °C annealed sample, but do not appear in the thermopower data for the 560 °C annealed sample, although the field-induced spin-flop transitions occur in both samples [35]. The small magnitude of both of these signals and their corresponding noise levels should be taken into consideration as a possible caveat. Also of note regarding the signal strength, the magnitude of the thermopower signal is an order of magnitude larger for the 320 °C sample for $T < T_{CDW}$, but is of a similar order of magnitude for $T > T_{CDW}$.

To understand the trend of the Nernst effect in this material and its dependence on annealing, fixed-temperature field sweeps were performed for several different temperatures. After deriving the raw Nernst signal $S_{xy}^0(H)$ from the raw signal, the signal was antisymmetrized according to $\frac{S_{xy}^0(H) - S_{xy}^0(-H)}{2}$, with H the applied magnetic field applied along the c -axis. This is done to isolate the true Nernst component of the signal and to remove any artifacts or contributions from the longitudinal voltage. The resulting Nernst effect signal S_{xy} for each of the annealing conditions is shown in Fig. 2b and Fig. 2d. Furthermore, the zero-field slope of $S_{xy} - \mu_0 H$ is defined as the Nernst coefficient ν , which will be discussed later.

The Nernst effect in both annealed samples has a generally linear trend, with some curvature appearing in the signal from the 320 °C annealed sample. Again, this curvature appears to correspond to the previously noted spin-flop features, and the slope has its largest magnitude around 40-45 K before gradually waning. This trend is notably absent in the 560 °C annealed sample signal, which does appear to have a maximum slope between 120 and 140 K, but then decreases in magnitude, and does not exhibit any other notable magnetic features. In addition to the general linear trend, the 320 °C signal also

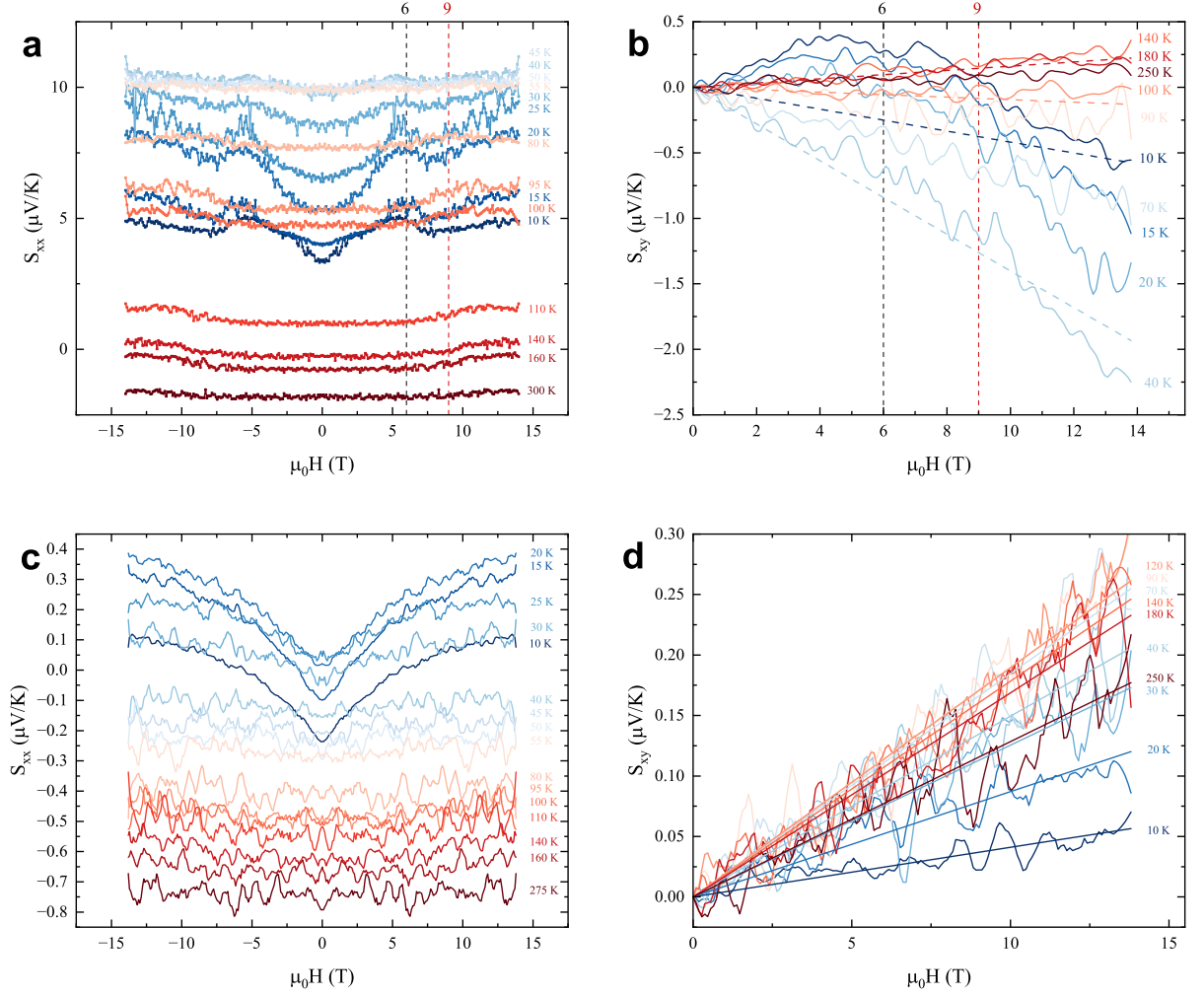


FIG. 2: (a, b) Thermopower signal S_{xx} and the Nernst signal S_{xy} of the 320 °C annealed sample as a function of the magnetic field at selected temperatures, along with selected linear fits as dotted lines. (c, d) Thermopower signal S_{xx} and the Nernst signal S_{xy} of the 560 °C annealed sample as a function of the magnetic field at selected temperatures, plotted alongside linear fits of the antisymmetrized transverse signal for clarity, as well as defining the Nernst coefficient ν .

exhibits a bump feature around 6 T, which is strongest between 40 and 45 K, and evolves with increasing temperature. This feature is likely a consequence of the 6 T spin-flop phase. However, as this signal is small, the noise is too prominent to see evidence of the 9 T spin-flop transition. The bump feature noted in the 320 °C sample does not appear to be present under the 560 °C annealing condition.

Further analysis of these trends can be observed in Fig. 3a, which displays the zero-field thermopower S_{xx} as a function of temperature for each annealing condition, and Fig. 3b, which shows ν for each annealing condition as a function of temperature. Both figures show

remarkably similar features in both S_{xx} and ν , with the 560 °C annealed sample remaining exclusively positive, and the 320 °C annealed sample changing sign close to $T = T_{CDW}$. Both of these samples share hole-like charge carriers at room temperature, which we define here as a positive Seebeck signal.

Furthermore, a rapid slope change appears to occur in the 320 °C annealed sample due to the charge density wave transition, and S_{xx} exhibits a kink feature at T_{CDW} , which we observe close to 105 K. This sign change is clearly absent in the sample annealed at 560 °C. In the CDW-containing sample, this trend continues for the temperature range $T_{CDW} < T < 300$ K that was mea-

sured. At $T < T_{CDW}$, the sample establishes much sizable negative (electron-like) thermopower signal, confirming that the dominant charge carriers are electrons for the CDW state. Holes become the dominant quasiparticle charge carriers around 130 K, when S_{xx} is positive in Fig. 3a.

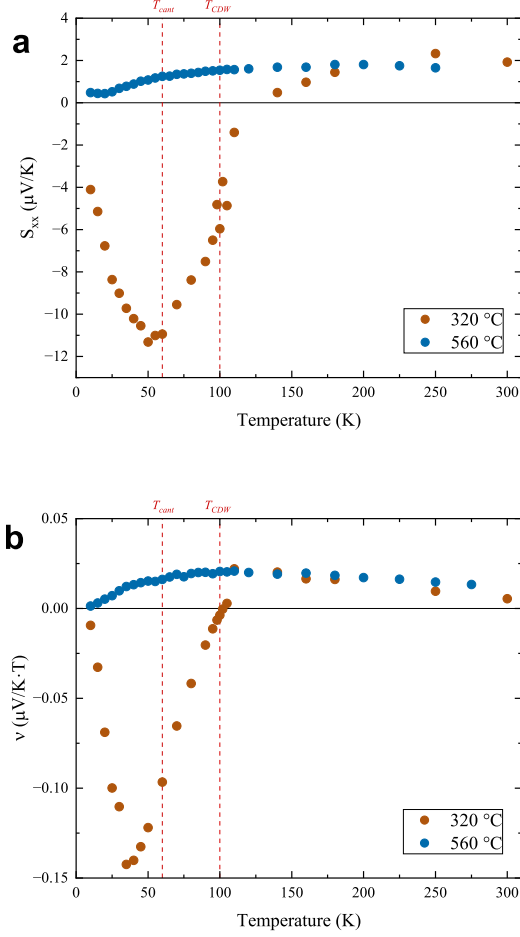


FIG. 3: (a) Seebeck coefficient S_{xx} and (b) Nernst coefficient ν for the 320 °C annealed sample (orange) and the 560 °C annealed sample (blue) in the magnetic field up to 14 T. The heat current is applied along the ab-plane, and the Seebeck data points were obtained from the zero-field ΔV value extracted from field sweeps at fixed temperatures, normalized by the sample geometry and the temperature difference across the sample.

Similarly, the Nernst coefficient ν established a similar trend in T . For $T < T_{CDW}$, the sample exhibiting the CDW shows a much more sizable Nernst coefficient in the opposite sign than that after the CDW transition. The Nernst coefficient ν - T is plotted in Fig. 3b. Notably, ν for the 320 °C annealed sample is significantly larger than that of the 560 °C annealed sample. This signal has a peak around 35-40 K, and changes sign around 105

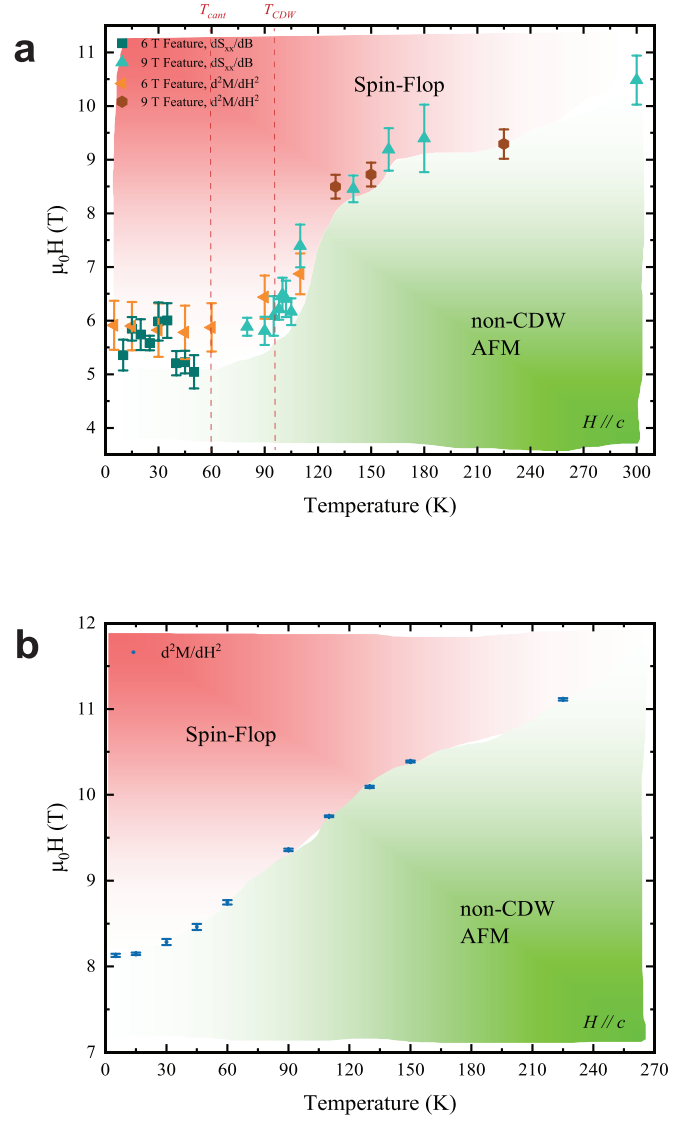


FIG. 4: The phase diagram of $\mu_0 H$ vs. T for (a) the 320 °C annealed sample and (b) the 560 °C annealed sample, using the locations of various magnetic features to define the phase transition. The boundaries of the canted AFM phase and CDW-ordered phase are delineated here as T_{cant} and T_{CDW} respectively.

K. We believe this sign change is further indicative of the CDW present in the 320 °C annealed sample and is again not present in ν for the 560 °C sample here. The absolute magnitude of the Nernst coefficient in the 320 °C annealed sample is almost 22x larger than the 560 °C sample at its largest magnitude as well. We also note that the 320 °C annealed sample has much stronger incommensurate magnetic peaks associated with spin density wave order below around 60 K that are considerably suppressed for the 560 °C annealed sample [35].

These findings are further examined in the phase diagrams seen in Fig. 4a and b. Regarding the 320 °C

annealed sample seen in Fig. 4a, there are two dM/dH peaks observed at 110 K, but only one peak for the temperatures both above and below 110 K (see the supplement for the magnetization $M - H$ data). This feature in addition to the Nernst sign change around 105 K both provide evidence for a spin-flop transition region between 105 and 110 K, near the CDW feature, consistent with previous work [35]. Previous works have also asserted the presence of incommensurate magnetic Bragg peaks around 60 K [21, 23, 32], which is also supported by our measurements and labeled here as T_{cant} . It is interesting to point out that recent photoemission work has also identified changes in the electronic structure at this characteristic temperature scale in the 320 °C annealed sample, while absent in the 560 °C annealed sample [25], consistent with the trends of S_{xx} and ν shown here.

In conclusion, in the Kagome metal FeGe, this thermoelectric effect study demonstrates a dramatic change in electronic structure accompanying the CDW transition. Compared to the crystal without the CDW transition, the crystal with the CDW is revealed to have a significantly enhanced Nernst effect and a dramatic sign change of the dominating carrier in the thermopower effect. This result suggests that the disorder created by the annealing conditions in Ge-1 site may prevent the CDW formation [35]. Thermoelectric effects are also shown to detect the spin-flop transition.

Acknowledgement. The work at the University of Michigan is supported by the National Science Foundation under Award No. DMR-2004288 and DMR-2317618 (transport measurements), by the Department of Energy under Award No. DE-SC0020184 (magnetization measurements) to Kuan-Wen Chen, Dechen Zhang, Guoxin Zheng, Aaron Chan, Yuan Zhu, Kaila Jenkins, and Lu Li. The single crystal synthesis and characterization at Rice are supported by US NSF DMR-2401084 and the Robert A. Welch Foundation under Grant No. C-1839 (P.D.).

* Electronic address: luli@umich.edu

- [1] T. M. Tritt, Thermal conductivity: theory, properties, and applications. Springer Science & Business Media (2005).
- [2] N. Nagaosa, J. Sinova, S. Onoda, A. H. MacDonald, and N. P. Ong, Anomalous Hall effect, *Rev. Mod. Phys.* 82, 1539 (2010).
- [3] S. Onoda, N. Sugimoto, and N. Nagaosa, Quantum transport theory of anomalous electric, thermoelectric, and thermal Hall effects in ferromagnets, *Phys. Rev. B* 77, 165103 (2008).
- [4] M. Ikhlas, T. Tomita, T. Koretsune, M.-T. Suzuki, D. Nishio-Hamane, R. Arita, Y. Otani, and S. Nakatsuji, Large anomalous Nernst effect at room temperature in a chiral antiferromagnet, *Nat. Phys.* 13, 1085–1090 (2017).
- [5] H. Yang, W. You, J. Wang, J. Huang, C. Xi, X. Xu, C. Cao, M. Tian, Z.-A. Xu, J. Dai, *et al.*, Giant anomalous Nernst effect in the magnetic Weyl semimetal $\text{Co}_3\text{Sn}_2\text{S}_2$, *Phys. Rev. Mater.* 4, 024202 (2020).
- [6] S. N. Guin, P. Vir, Y. Zhang, N. Kumar, S. J. Watzman, C. Fu, E. Liu, K. Manna, W. Schnelle, J. Gooth, *et al.*, Zero-Field Nernst Effect in a Ferromagnetic Kagome-Lattice Weyl-Semimetal $\text{Co}_3\text{Sn}_2\text{S}_2$, *Adv. Mater.* 31, 1806622 (2019).
- [7] R. P. Madhugaria, S. Mozaffari, H. Zhang, W. R. Meier, S.-H. Do, R. Xue, T. Matsuoka, and D. G. Mandrus, Topological Nernst and topological thermal Hall effect in rare-earth kagome ScMn_6Sn_6 , *Phys. Rev. B* 108, 125114 (2023).
- [8] H. Zhang, C. Q. Xu, and X. Ke, Topological Nernst effect, anomalous Nernst effect, and anomalous thermal Hall effect in the Dirac semimetal Fe_3Sn_2 , *Phys. Rev. B* 103, L201101 (2021).
- [9] K. Behnia, The Nernst effect and the boundaries of the Fermi liquid picture, *J. Phys.: Condensed Matter* 21, 113101 (2009).
- [10] K. Behnia and H. Aubin, Nernst effect in metals and superconductors: a review of concepts and experiments, *Rep. Prog. Phys.* 79, 046502 (2016).
- [11] E.H. Sondheimer, The Theory of the Galvanomagnetic and Thermomagnetic Effects in Metals, *Proceedings of the Royal Society of London. Series A, Mathematical and Physical Sciences* 193(1035), 484-512 (1948).
- [12] Z. Zhu, H. Yang, B. Fauque, Y. Kopelevich, and K. Behnia, Nernst effect and dimensionality in the quantum limit, *Nat. Phys.* 6, 26-29 (2010).
- [13] Y. Wang, L. Li, and N. P. Ong, Nernst effect in high- T_c superconductors, *Phys. Rev. B* 73 (2), 024510 (2006).
- [14] Y. Onose, L. Li, C. Petrovic and N. P. Ong, Anomalous thermopower and Nernst effect in CeCoIn_5 : Loss of entropy current in precursor state, *Europhysics Letters Association* 79 (1), 17006 (2007).
- [15] L. Chen, Z. Xiang, C. Tinsman, B. Lei, X. Chen, G. D. Gu, and L. Li, Spontaneous Nernst effect in the iron-based superconductor $\text{Fe}_{1+y}\text{Te}_{1-x}\text{Se}_x$, *Phys. Rev. B* 102, 054503 (2020).
- [16] J. M. Ziman, *Electrons and Phonons: The Theory of Transport Phenomena in Solids*, Oxford University Press; Reprint edition, (2001).
- [17] K. Behnia, *Fundamentals of Thermoelectricity*, Oxford: Oxford University Press. (2015).
- [18] Y.-X. Jiang, J.-X. Yin, M.M. Denner, N. Shumiya, B.R. Ortiz, G. Xu, Z. Guguchia, J. He, M.S. Hossain, X. Liu, J. Ruff, L. Kautzsch, S.S. Zhang, G. Chang, I. Belopolski, Q. Zhang, T.A. Cochran, D. Multer, M. Litskevich, Z.-J. Chang, X.P. Yang, Z. Wang, R. Thomale, T. Neupert, S.D. Wilson, and M.Z. Hasan, Unconventional chiral charge order in kagome superconductor KV_3Sb_5 , *Nature Materials* 20, 1353-1357 (2021).
- [19] X. Xu, J. Yin, Z. Qu, and S. Jia, Quantum interactions in topological R166 kagome magnet, *Rep. Prog. Phys.* 86, 11 (2023).
- [20] P. Sun and F. Steglich, Nernst Effect: Evidence of Local Kondo Scattering in Heavy Fermions, *Phys. Rev. Lett.* 110, 216408 (2013).
- [21] X. Teng, L. Chen, F. Ye, E. Rosenberg, Z. Liu, J.X. Yin, Y.-X. Jiang, J.S. Oh, M.Z. Hasan, K. Neubauer, B. Gao, Y. Xie, M. Hashimoto, D. Lu, C. Jozwiak, A. Bostwick, E. Rotenberg, R.J. Burgeneau, J.-H. Chu, M. Yi, and P. Dai, Discovery of charge density wave in a kagome

- lattice antiferromagnet, *Nature* 609, 490-495(2022).
- [22] Jia-Xin Yin, Yu-Xiao Jiang, Xiaokun Teng, Md Shafayat Hossain, Sougata Mardanya, Tay-Rong Chang, Zijin Ye, Gang Xu, M Michael Denner, Titus Neupert, Benjamin Lienhard, Han-Bin Deng, Chandan Setty, Qimiao Si, Guoqing Chang, Zurab Guguchia, Bin Gao, Nana Shumiya, Qi Zhang, Tyler A Cochran, Daniel Multer, Ming Yi, Pengcheng Dai, M Zahid Hasan, Discovery of charge order and corresponding edge state in kagome magnet FeGe, *Phys. Rev. Lett.* 129, 166401 (2022).
- [23] X. Teng, J.S. Oh, H. Tan, L. Chen, J. Huang, B. Gao, J.X. Yin, J.-H. Chu, M. Hashimoto, D. Lu, C. Jozwiak, A. Bostwick, E. Rotenberg, G. Granroth, B. Yan, R.J. Burgeneau, P. Dai, and M. Yi, Magnetism and charge density wave order in Kagome FeGe, *Nat. Phys.* 19, 814-822 (2023).
- [24] S. Shao, J.-X. Yin, I. Belopolski, J.-Y. You, T. Hou, H. Chen, Y. Juang, M.S. Hossain, M. Yahyavi, C.-H. Hsu, Y.P. Feng, A. Bansil, M.Z. Hasan, and G. Chang, Intertwining of Magnetism and Charge Ordering in Kagome FeGe, *ACS Nano* 17, 10164-10171 (2023).
- [25] J. Oh, A. Biswas, M. Klemm, H. Tan, Y. Xie, B. Gao, M. Hashimoto, D. Lu, B. Yan, P. Dai, R. J. Birgeneau, M. Yi, Disentangling the intertwined orders in a magnetic kagome metal, *Sci. Adv.* 11, eadt2195 (2025).
- [26] Z. Zhao, T. Li, P. Li, X. Wu, J. Yao, Z. Chen, S. Cui, Z. Sun, Y. Yang, Z. Jiang, Z. Liu, A. Louat, T. Kim, C. Cacho, A. Wang, Y. Wang, D. Shen, J. Jiang, D.L. Feng, Photoemission Evidence of a Novel Charge Order in Kagome Metal FeGe, *Science China Physics, Mechanics & Astronomy* 68, 267012 (2025).
- [27] Xiaokun Teng, David W. Tam, Lebing Chen, Hengxin Tan, Yaofeng Xie, Bin Gao, Garrett E. Granroth, Alexandre Ivanov, Philippe Bourges, Binghai Yan, Ming Yi, and Pengcheng Dai, Spin-Charge-Lattice Coupling across the Charge Density Wave Transition in a Kagome Lattice Antiferromagnet, *Phys. Rev. Lett.* 133, 046502 (2024).
- [28] D.S. Bouma, Z. Chen, B. Zhang, F. Bruni, M.E. Flatté, A. Ceballos, R. Streubel, L.-W. Wang, R.Q. Wu, and F. Hellman, Itinerant ferromagnetism and intrinsic anomalous Hall effect in amorphous iron-germanium, *Phys. Rev. B* 101, 014402 (2020).
- [29] N.A. Porter, J.C. Gartside, and C.H. Marrows, Scattering mechanisms in textured FeGe thin films: Magnetoresistance and the anomalous Hall effect, *Phys. Rev. B* 90, 024403 (2014).
- [30] J. Bernhard, B. Lebech, and O. Beckman, Neutron diffraction studies of the low-temperature magnetic structure of hexagonal FeGe, *J. Phys. F: Met. Phys.* 14, 2379 (1984).
- [31] Lebing Chen, Xiaokun Teng, Hengxin Tan, Barry L. Winn, Garrett E. Granroth, Feng Ye, D. H. Yu, R. A. Mole, Bin Gao, Binghai Yan, Ming Yi, and Pengcheng Dai, Competing itinerant and local spin interactions in kagome metal FeGe, *Nature Communications* 15, 1918 (2024).
- [32] X. Wu, X. Mi, L. Zhang, C.-W. Wang, N. Maraytta, X. Zhou, M. He, M. Merz, Y. Chai, and A. Wang, Annealing-tunable charge density wave in the kagome antiferromagnet FeGe, *Phys. Rev. Lett.* 132, 256501 (2024).
- [33] Ziyuan Chen, Xueliang Wu, Shiming Zhou, Jiakang Zhang, Ruotong Yin, Yuanji Li, Mingzhe Li, Jiashuo Gong, Mingquan He, Yisheng Chai, Xiaoyuan Zhou, Yilin Wang, Aifeng Wang, Ya-Jun Yan, and Dong-Lai Feng, Discovery of a long-ranged charge order with 1/4 Ge1-dimerization in an antiferromagnetic Kagome metal, *Nature Communications* 15, 6262 (2024).
- [34] C. Shi, Y. Liu, B.B. Maity, Q. Wang, S.R. Kotla, S. Ramakrishnan, C. Eisele, H. Agarwal, L. Noohinejad, Q. Tao, B. Kang, Z. Lou, X. Yang, Y. Qi, X. Lin, Z.-A. Xu, A. Thamizhavel, G.-H. Cao, S. van Smaalen, S. Cao, and J.-K. Bao, Annealing-induced long-range charge density wave order in magnetic kagome FeGe: Fluctuations and disordered structure, *Science China* 67(11), 117012 (2024).
- [35] M. Klemm, S. Siddique, Y.-C. Chang, S. Xu, Y. Xie, T. Legvold, M.T. Kiani, F. Ye, H. Cao, Y. Hao, W. Tian, H. Luetkens, M. Matsuda, D. Natelson, Z. Guguchia, C.-L. Huang, M. Yi, J.J. Cha, and P. Dai, Vacancy-induced suppression of CDW order and its impact on magnetic order in kagome antiferromagnet FeGe, *Nature Communications* 16, 3313 (2025).
- [36] Y. Zhu, D. Zhang, G. Zheng, K.-W. Chen, H. Bhandari, K. Jenkins, A. Chan, N. J. Ghimire, and L. Li, Geometrical Nernst effect in the kagome magnet $\text{YMn}_6\text{Sn}_4\text{Ge}_2$, *Phys. Rev. B* 110(19), 195125 (2024).
- [37] T. Asaba, V. Ivanov, S. M. Thomas, S.Y. Savrasov, J.D. Thompson, E.D. Bauer, and F. Ronning, Colossal anomalous Nernst effect in a correlated noncentrosymmetric kagome ferromagnet, *Sci. Adv.* 7, eabf1467 (2021).
- [38] S. Roychowdhury, A. M. Ochs, S. N. Guin, K. Samanta, J. Noky, C. Shekhar, M. G. Vergniory, J. E. Goldberger, and C. Felser, Large room temperature anomalous transverse thermoelectric effect in kagome antiferromagnet YMn_6Sn_6 , *Adv. Mater.* 34, 2201350 (2022).
- [39] H. Bhandari, R. L. Dally, P. E. Siegfried, R. B. Regmi, K. C. Rule, S. Chi, J. W. Lynn, I. Mazin, and N. J. Ghimire, Magnetism and fermiology of kagome magnet $\text{YMn}_6\text{Sn}_4\text{Ge}_2$, *npj Quantum Materials* 9, 6 (2024).
- [40] C. Zeng, X.-Q. Yu, Z.-M. Yu, and Y. Yao, Band tilt induced nonlinear Nernst effect in topological insulators: An efficient generation of high-performance spin polarization, *Phys. Rev. B* 106, L081121 (2022).
- [41] M. Ceccardi, A. Zeugner, C. Hess, B. Büchner, D. Marré, A. Isaeva, and F. Caglieris, Anomalous Nernst effect in the topological and magnetic material MnBi_4Te_7 , *npj Quantum Materials* 8(76), (2023).
- [42] G. Sharma, Tunable topological Nernst effect in two-dimensional transition-metal dichalcogenides, *Phys. Rev. B* 98, 075416 (2018).
- [43] W.-L. Lee, S. Watauchi, V.L. Miller, R.J. Cava, and N.P. Ong, Anomalous Hall Heat Current and Nernst Effect in the $\text{CuCr}_2\text{Se}_{4-x}\text{Br}_x$ Ferromagnet, *Phys. Rev. Lett.* 93, 226601 (2004).
- [44] T. Miyasato, N. Abe, T. Fujii, A. Asamitsu, S. Onoda, Y. Onose, N. Nagaosa, and Y. Tokura, Crossover Behavior of the Anomalous Hall Effect and Anomalous Nernst Effect in Itinerant Ferromagnets, *Phys. Rev. Lett.* 99, 086602 (2007).
- [45] Y. Pu, D. Chiba, F. Matsukura, H. Ohno, and J. Shi, Mott Relation for Anomalous Hall and Nernst Effects in $\text{Ga}_{1-x}\text{Mn}_x\text{As}$ Ferromagnetic Semiconductors, *Phys. Rev. Lett.* 101, 117208 (2008).
- [46] T.-C. Chuang, P.L. Su, P. Wu, and S. Y. Huang, Enhancement of the anomalous Nernst effect in ferromagnetic thin films, *Phys. Rev. B* 96, 174406 (2017).
- [47] R. Ramos, M.H. Aguirre, A. Anadón, J. Blasco, I. Lucas,

- K. Uchida, P.A. Algarabel, L. Morellón, E. Saitoh, and M.R. Ibarra, Anomalous Nernst effect of Fe_3O_4 single crystal, *Phys. Rev. B* 90, 054422 (2014).
- [48] G. Sharma, C. Moore, S. Saha, and S. Tewari, Nernst effect in Dirac and inversion-asymmetric Weyl semimetals, *Phys. Rev. B* 96, 195119 (2017).
- [49] S. Watzman, T.M. McCormick, C. Shekhar, S.-C. Wu, Y. Sun, A. Prakash, C. Felser, N. Trivedi, and J.P. Heremans, Dirac dispersion generates unusually large Nernst effect in Weyl semimetals, *Phys. Rev. B* 97, 161404(R) (2018).
- [50] L. Xu, X. Li, L. Ding, T. Chen, A. Sakai, B. Fauqué, S. Nakatsuji, Z. Zhu, and K. Behnia, Anomalous transverse response of Co_2MnGa and universality of the room-temperature $\alpha_{ij}^A/\sigma_{ij}^A$ ratio across topological magnets, *Phys. Rev. B* 101, 180404 (2020).
- [51] L. Ding, J. Koo, L. Xu, X. Li, X. Lu, L. Zhao, Q. Wang, Q. Yin, H. Lei, B. Yan, Z. Zhu, and K. Behnia, Intrinsic anomalous Nernst effect amplified by disorder in a half-metallic semimetal, *Phys. Rev. X* 9, 041061, (2019).